北見工業大学研究報告
第21巻 第1号 (平成元年)

Memoirs of the Kitami Institute of Technology
Vol. 21 No. 1 (1989)

Interpretation of the Multiplicity of Kinetics in Heterogeneous Catalysis*

by Hiroshi TAKEDA**, Tohru KANNO*** and Masayoshi KOBAYASHI***

(Received April 27, 1989)

1. Abstract

The multiplicity of reaction kinetics in heterogeneous catalysis has been studied by using the oxidation of propene over Pt/SiO_2 of widely varying dispersion, relating to the adsorption behavior of reaction components at temperature a range of 290~350°C. The reaction consists of a partial oxidation to propanal and complete oxidation to CO_2 and H_2O, each of which progresses independently in parallel on own active sites.

The rate of propanal formation indicates a characteristic oscillation. The oscillation seems to be a multiplicity caused by the switching between two different surface structures on each of which the partial oxidation progresses at different rate, high rate ($r_{CHO}{}^{H}$) and low rate ($r_{CHO}{}^{L}$). For $r_{CHO}{}^{H}$ and $r_{CHO}{}^{L}$, the L-H and E-R models consistently explained all experimental data. Three rate equations for the two rates to form propanal and the complete oxidation are expressed

$$r_{CHO}{}^{H} = k_{CHO}{}^{H} P_{C_3H_6}{}^{0.25} P_{N_2O}{}^{0.42}$$

$$r^{CHOL} = k_{CHO}{}^{L} P_{C_3H_6}{}^{0.29} P_{N_2O}{}^{0.31}$$

$$r_{CO_2} = k_{CO_2} P_{C_3H_6}{}^{0.36} P_{N_2O}{}^{0.81}$$

The activation energies for propanal formation at high and low rates and for CO_2 formation were evaluated to be 9(±4) kJ/mol 92~218 kJ/mol and 85(±5) kJ/mol, respectively. All the surface coverages of N_2O, C_3H_6 and propanal during the reaction were evaluated to be $\theta_{N_2O}=0.13$, $\theta_{C_3H_6}=0.69-1.17$ and $\theta_{CHO}=0.15$, respectively. $\theta_{C_3H_6}$ is presumed to be a sort of trigger for the oscillating rate.

2. Introduction

Generally speaking, the rate and product distribution in hererogeneously catalysed reactions are sensitively influenced by the particle sizes loaded on supports. Boudart[1] classified the catalytic reactions as two groups such as structure sensitive and structure insensitive. For the first one, alkane hydrogenolysis[2] and isomerization[3] on platinum catalysts were taken and, for the second one, cyclopropane ring opening[4] and olefin hydrogenation[5] were taken. Recently, Somorjai and Carrazza[6] reviewed the structure sensitivity of catalytic reactions and classified

Department of Industrial Chemistry, Kitami Institute of Technology, Kitami, Hokkaido 090, Japan.

* This paper was party presented at the 11th Iberoamerican Symposium on Catalysis in 1988.

** Department of Chemical Environmental Engineering.

*** Department of Industrial Chemistry.

them into three groups as type I : structure-insensitive reactions, type II : structure-sensitive reactions and type III : reactions that show both behaviors depending on the experimental conditions. For type I, they explained it as the presence of adsorbed species on the surface that either weaken the reactant-catalyst surface interaction or are inactive in the reaction, such as ethylene hydrogenation over Pt and Rh (111) single-crystal surfaces[7] and cyclohexene hydrogenation over Pt[8] and Pt/SiO_2[9].

For type II, since the relative concentrations of terraces, steps and kinks change with catalyst particle size, one may presume thereby that variations of adsorbate bond strengths due to changes in local atomic structure are responsible for the modification of reaction rates[6]. The synthesis of ammonia exhibits the greatest structure sensitivity on iron and rhenium.[10,11,12] In the case of iron, the Fe (110) face which is the closest packed surface structure has the lowest activity of ammonia synthesis. The Fe (100) face which is a more open surface has 25 times the activity of the Fe (110) face. The Fe (111) face which is the most open surface structure has the highest activity[6].

For the type III, The oxidation of carbon monoxide on some transition metals was chosen. When a high partial pressure of carbon monoxide ($P_{CO}/P_{total}>0.01$) is chosen on supported platinum, the reaction is structure insensitive. If the partial pressure of carbon monoxide is chosen as low as $P_{CO}/P_{total}<0.004$, the reaction is structure sensitive ; the T. O. F increases with the particle size of the catalyst. These results from the shift of the rate-determining step caused by variations in the amounts and/or the form of species adsorbed on the surface depend on the reaction conditions.

In the present study, our interest is focused on the oscillating kinetics in heterogeneous catalysis caused by the mobile metal atoms on the surface and the structure sensitivity of the kinetics depending on the reconstruction of the surface layer. To analyse the transient behavior of oscillatory behavior, the transient response method[13,14] is employed.

3. Experimental Methods

The experimental apparatus[15,16] and the platinum catalyst preparation and characterization procedures are described in detail elsewhere[17,18]. All the catalysts used in this study were kindly supplied by Professor Burwell, Jr. of Northwestern University[17,18]. Platinum was supported on silica gel by both an ion exchange and an impregnation techniques. The dispersion of platinum was measured by both the chemisorbed amount of hydrogen and X-ray diffraction analysis, evaluating to be Dh=7, 16, 27, 40 and 81%[15~18]. The particle sizes for Dh=7, 27 and 40 were 80~130, 30~40 and 20~30 Å respectively. For Dh=81 and 16%, Yacaman et al's procedure[19] was applied and evaluated to be about 14 and 60 Å, respectively. The amounts of platinum loaded were 0.825 for Dh=81%, 1.10 for Dh=40%, 1.50 for 27%, 1.48 for Dh=16% and 1.91 wt% for Dh=17%. The silica gel used as a support was prepared from Davison Grade 62 and had

a BET surface area of 285 m^2/g, the mean pore diameter was 140 Å and the pore volume was 1.2 cm^3/g.

Prior to use for propene oxidation, the catalyst was treated in a pure He stream at 300°C for 12 hr to clean the surface for adsorption. The amount of the catalyst including support to pack into the reactor was adjusted to satisfy the differential reactor with the total conversion less than 10%, 1.76 g for Dh=81%, 1.00 g for Dh=40%, 2.09 g for Dh=27%, 1.88 g for Dh=16% and 2.35 g for Dh=7%. The lengths of catalyst beds were 13.0, 8.4, 14.3, 12.5 and 16.0 cm respectively.

A tubular flow reactor which was made of a Pyrex glass tube of 0.7~1.0 cm ID and 80 cm length was used. The reactor was immersed in a fluidized sand bath the temperature of which was carefully controlled to an accuracy of ±1°C. A thermocouple of chromel-alumel of 0.1 mm O. D., which was covered by an insulator of I=1.0 mm, was inserted into the catalyst bed directly. This could detect the temperature fluctuation in the catalyst bed with great sensitivity.

The total flow rate used was 60~320 ml/min and the gas composition was changed by varying the concentration of helium as a balance gas, with no change in the flow rate. The gas composition was switched between three different flow systems each of which had a different gas composition, by using two four way valves. The accuracy of the flow rate at the step change was within ±5% of total flow rate.

All gas components in the effluent streams were analysed by two gas chromatographs. A Porapak Q columm (3 m) was used to analyse C_3H_6, N_2O, CO_2, H_2O and propanal, and Molecular Sieves 13X (2 m) to analyse N_2, CO and O_2. The gas analysis was done every 15 sec by using an one-ml syringe. When the transient response was too fast to follow, the same transient response was repeated a few times and the results were superimposed to draw the response curve as continuously as possible.

The external particle and intraparticle mass transfer effects were reconfirmed to be negligible by using Weisz and Prater's criteria assuming first order reactions[20].

$$\Phi = \frac{r R_p^2}{\mathrm{Co}\, D_{\mathrm{eff}}} \qquad (1)$$

where r is the observed rate of reaction per unit volume of the catalyst layer, R_p is particle radius, Co is concentration of reaction component i. In the present case, one may use $R_p=0.04$ cm, $r=2.53\times10^{-9}$ mol/cm^3·sec, $\mathrm{Co}=1.66\times10^{-4}$ mol/cm^3, $D_{\mathrm{eff}}=1.64\times10^{-3}$ cm^2/sec and calculated to be $I=3.72\times10^{-3}\ll1$. Based on these results, the intraparticle diffusion effect should be neglected.

4. Experimental Results and Discussion

4-1. Adsorption Behavior of Gases on Silica Gel Support

The surface coverage of reaction components is one of the important parameters in controlling the oscillatory behavior[6]. In this section, the adsorption and

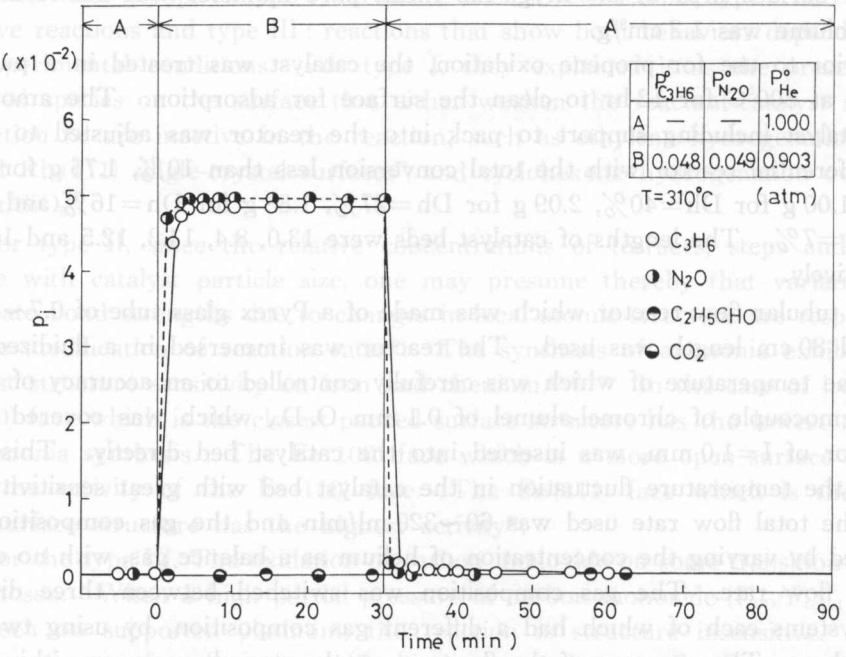

	$P^{\circ}_{C_3H_6}$	$P^{\circ}_{N_2O}$	P°_{He}
A	—	—	1.000
B	0.048	0.049	0.903

Fig. 1. Adsorption and desorption behavior of C_3H_6, N_2O, C_2H_5CHO and CO_2 on SiO_2. Gas composition; Run A: $P_{He}=1.00$ atm, Run B: $P_{C_3H_6}=0.05$, $P_{N_2O}=0.05$ and $P_{He}=0.90$ atm. $T=310°C$, $F=80$ ml/min.

desorption behavior of all the components on silica gel alone are revealed in detail and the results obtained were presented in Fig. 1. The response curves of propene and nitrous oxide show a delay, exhibiting their adsorption on the silica gel. The desorption curves of the two gases in Run 3 can be graphically integrated to evaluate the amounts of reversibly adsorbed ones, as $q_{N_2O}=1.02\times 10^{-4}$ mol/g-SiO_2 and $q_{C_3H_6}=1.91\times 10^{-4}$ mol/g-SiO_2. No CO_2 and propanal were formed through all experimental conditions indicating no reactivity of the silica gel support.

4-2. Adsorption and Desorption Behavior of Gases on Pt/SiO_2

The oxidation of C_3H_6 by N_2O progresses at temperatures higher than 290°C and produces CO_2, H_2O, propanal and a little amount of propane which is less than 5% of the total products. In addition, the oscillatory rate of propanal appears in the specified reaction conditions depending on Dh and $P_{C_3H_6}/P_{N_2O}$ $(=R)$ ratio.

Let us consider the no-oscillation region at $R>P_{C_3H_6}/P_{N_2O}=0.8$ and evaluate the amounts of adsorbed N_2O, C_3H_6, CO_2 and propanal. Fig. 2 illustrates the adsorption and desorption response curves of the reaction components all of which show a delay. The graphical integration of the curves (see shaded area) in Runs 2 and 3 gives the adsorbed (q_{ad}) and desorbed amounts (q_{des}) respectively.

The correct amount of adsorbed propanal is difficult to evaluate because it

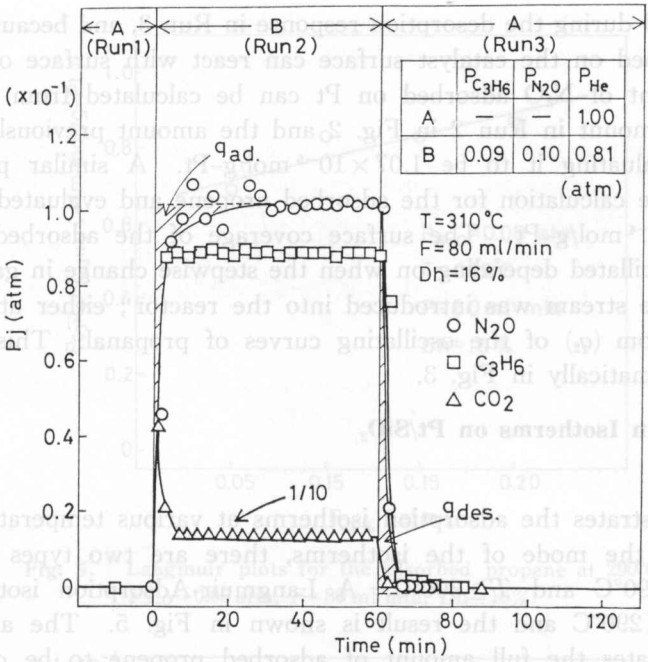

	$P_{C_3H_6}$	P_{N_2O}	P_{He}
A	—	—	1.00
B	0.09	0.10	0.81

(atm)

Fig. 2. Transient behavior of reaction components caused by the stepwise change in gas composition. Gas composition; Run A: $P_{He}=1.00$ atm, Run B: $P_{C_3H_6}=0.09$, $P_{N_2O}=0.10$ and $P_{He}=0.81$ atm. $T=310°C$, $F=80$ ml/min, Dh=16%.

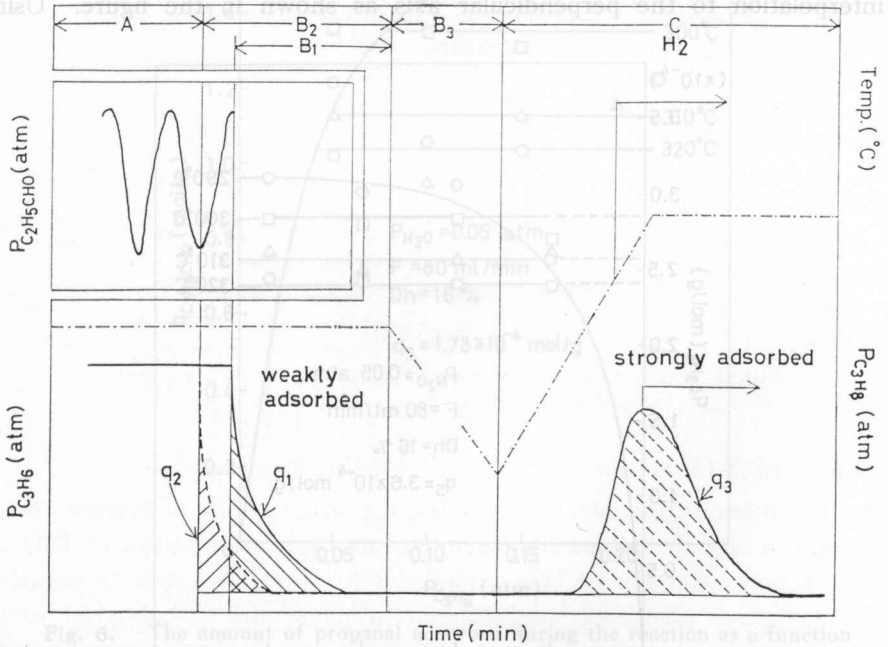

Fig. 3. Schematic explanation of how the amounts of weakly and strongly adsorbed propene during the reaction can be estimated. q_1 is the weakly adsorbed one at the peak of oscillating propanal. q_2 is the weakly adsorbed one at the bottom of oscillating propanal. q_3 is the amount of strongly adsorbed propene which desorbs as propane according to the reaction of the strongly adsorbed propene with H_2.

is still produced during the desorption response in Run 3, and because the residual propene adsorbed on the catalyst surface can react with surface oxygen in Run 3. The amount of N_2O adsorbed on Pt can be calculated from the difference between the amount in Run 2 in Fig. 2 and the amount previously obtained on silica only, evaluating it to be 1.07×10^{-5} mol/g-Pt. A similar procedure was applied into the calculation for the adsorbed propene and evaluated to be ranged $6.56\sim9.84\times10^{-4}$ mol/g-Pt. The surface coverage of the adsorbed propene obtained thus, oscillated depending on when the stepwise change in gas composition to the pure He stream was introduced into the reactor; either at the peak (q_1) or at the bottom (q_2) of the oscillating curves of propanal. This procedure is explained schematically in Fig. 3.

4-3. Adsorption Isotherms on Pt/SiO_2

(1) Propene

Fig. 4 illustrates the adsorption isotherms at various temperatures. As can be seen from the mode of the isotherms, there are two types of adsorption between $T\leq290$°C and $T\geq300$°C. A Langmuir-Adsorption isotherm can be applied at $T\leq290$°C and the result is shown in Fig. 5. The analysis of the isotherm evaluates the full amount of adsorbed propene to be $q_m=3.60\times10^{-4}$ mol/g-Pt. The full amounts at 300, 310 and 320°C, on the other hand can be evaluated to be 2.81×10^{-4}, 2.59×10^{-4} and 2.45×10^{-4} mol/g-Pt respectively, by the interpolation to the perpendicular axis as shown in the figure. Using q_m

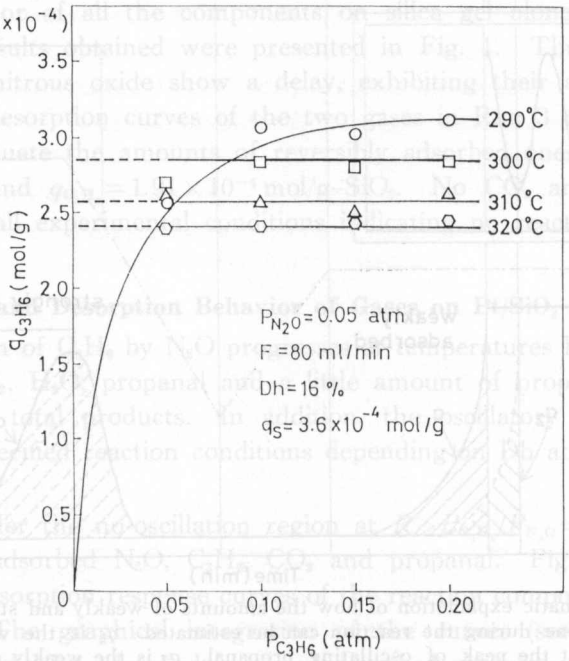

Fig. 4. Adsorption isotherms of propene at various temperatures during the reaction. $P_{N_2O}=0.05$ atm, $F=80$ ml/min, Dh=16%.

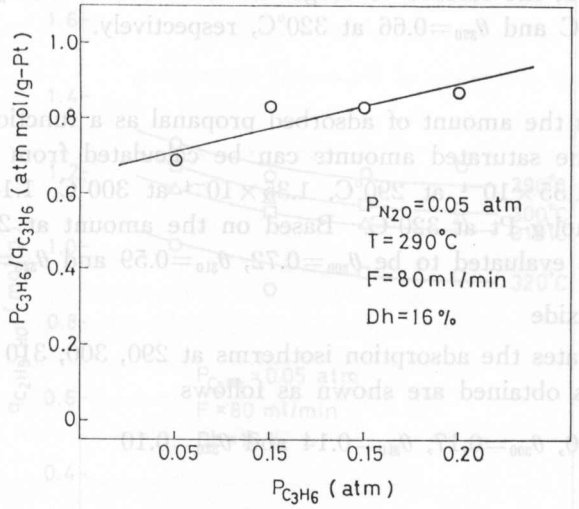

Fig. 5. Langmuir plots for the adsorbed propene at 290°C. $P_{N_2O}=0.05$ atm, $F=80$ ml/min, Dh=16%.

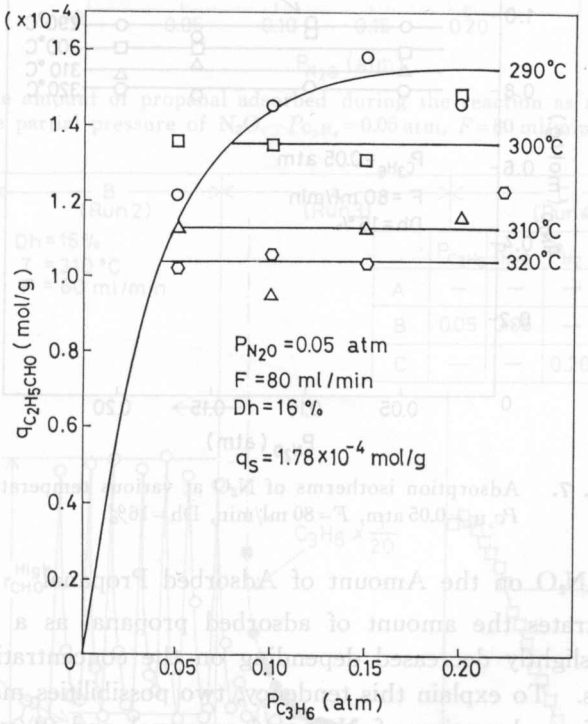

Fig. 6. The amount of propanal adsorbed during the reaction as a function of the partial pressure of propene. $P_{N_2O}=0.05$ atm, $F=80$ ml/min, Dh=16%.

evaluated at 290°C, the surface coverages are calculated to be $\theta_{300}=0.82$ at 300°C, $\theta_{310}=0.72$ at 310°C and $\theta_{320}=0.66$ at 320°C, respectively.

(2) Propanal

Fig. 6 shows the amount of adsorbed propanal as a function of $P_{C_3H_6}$ during the reaction. The saturated amounts can be calculated from the interporation of the curves ; 1.55×10^{-4} at 290°C, 1.35×10^{-4} at 300°C, 1.14×10^{-4} at 310°C and 1.03×10^{-4} mol/g-Pt at 320°C. Based on the amount at 290°C, the surface coverage may be evaluated to be $\theta_{300}=0.72$, $\theta_{310}=0.59$ and $\theta_{320}=0.51$.

(3) Nitrous Oxide

Fig. 7 illustrates the adsorption isotherms at 290, 300, 310 and 320°C. The surface coverages obtained are shown as follows

$$\theta_{290}=0.20,\ \theta_{300}=0.17,\ \theta_{310}=0.14 \text{ and } \theta_{320}=0.10$$

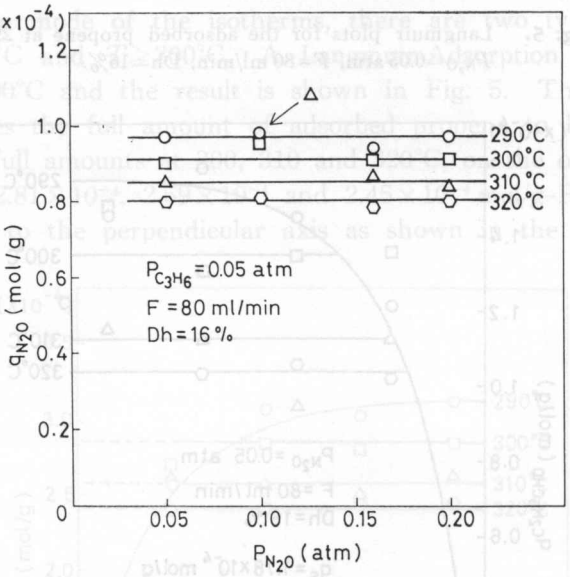

Fig. 7. Adsorption isotherms of N_2O at various temperatures. $P_{C_3H_6}=0.05$ atm, $F=80$ ml/min, Dh=16%.

(4) Effect of N_2O on the Amount of Adsorbed Propanal

Fig. 8 illustrates the amount of adsorbed propanal as a function of P_{N_2O}. The amount is slightly decreased depending on the concentration of N_2O at all the temperatures. To explain this tendency, two possibilities may be considered ; (1) the competitive adsorption of N_2O and propanal and (2) adsorbed propanal being consumed by the consecutive oxidation due to the surface oxygen species supplied from gaseous N_2O. The rate of complete oxidation into CO_2 and H_2O, on the other hand, is 0.81 order with respect to the concentration of N_2O which is about two times larger than the one for propene. These contrasting results

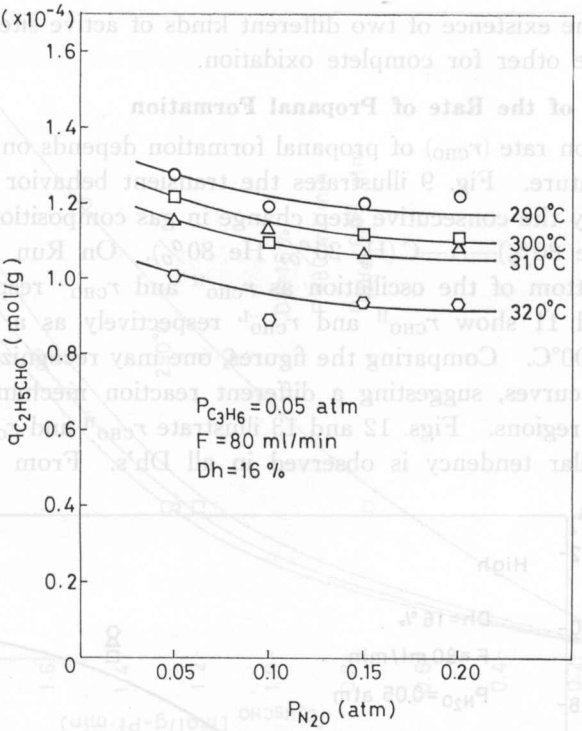

Fig. 8. The amount of propanal adsorbed during the reaction as a function of the partial pressure of N_2O. $P_{C_3H_6}=0.05$ atm, $F=80$ ml/min, Dh=16%.

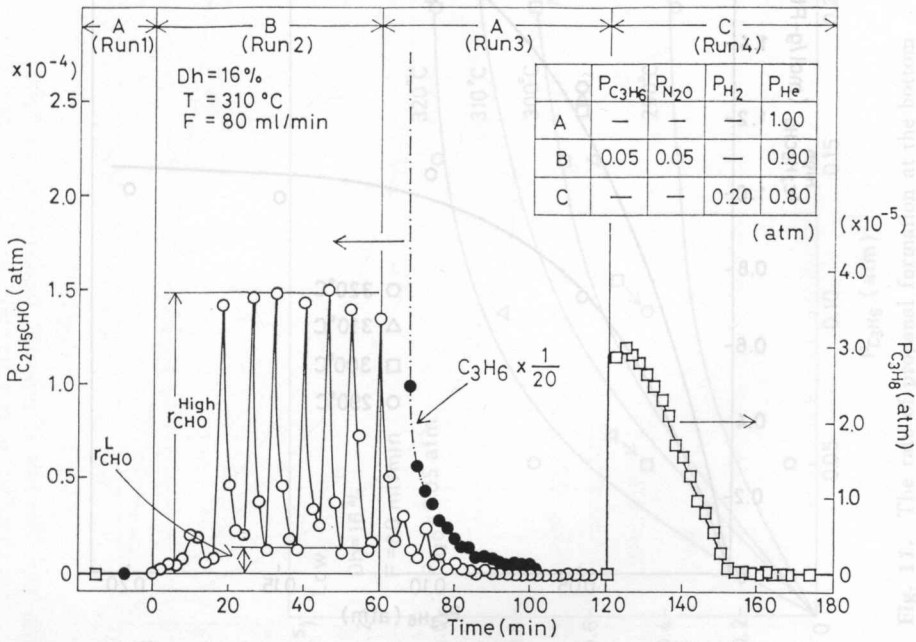

Fig. 9. Transient behavior of propanal, propene and propane caused by the consecutive step change in gas composition A (He 100%)—B (C_3H_6 20%, He 80%)—A—C (H_2 20%, He 80%). $T=310$°C, $F=80$ ml/min, Dh=16%. $r_{CHO}{}^{H}$ is the rate of propanal formation at the peak of oscillation and $r_{CHO}{}^{L}$ is at the bottom of oscillation.

clearly propose the existence of two different kinds of active sites: one for partial oxidation and the other for complete oxidation.

4-4. Multiplicity of the Rate of Propanal Formation

The oscillation rate (r_{CHO}) of propanal formation depends on the gas composition and temperature. Fig. 9 illustrates the transient behavior of reaction components caused by the consecutive step change in gas composition A (He 100%)—B (C_3H_6 20%, He 80%)—A—C (H_2 20%, He 80%). On Run 2, one designates the peak and bottom of the oscillation as $r_{CHO}{}^{H}$ and $r_{CHO}{}^{L}$ respectively (see Fig. 9). Figs. 10 and 11 show $r_{CHO}{}^{H}$ and $r_{CHO}{}^{L}$ respectively as a function of $P_{C_3H_6}$ at 290 and $T>300$°C. Comparing the figures, one may recognize clear differences in the mode of curves, suggesting a different reaction mechanism between the two temperature regions. Figs. 12 and 13 illustrate $r_{CHO}{}^{H}$ and $r_{CHO}{}^{L}$, as a function of P_{N_2O}. A similar tendency is observed in all Dh's. From the mode of the

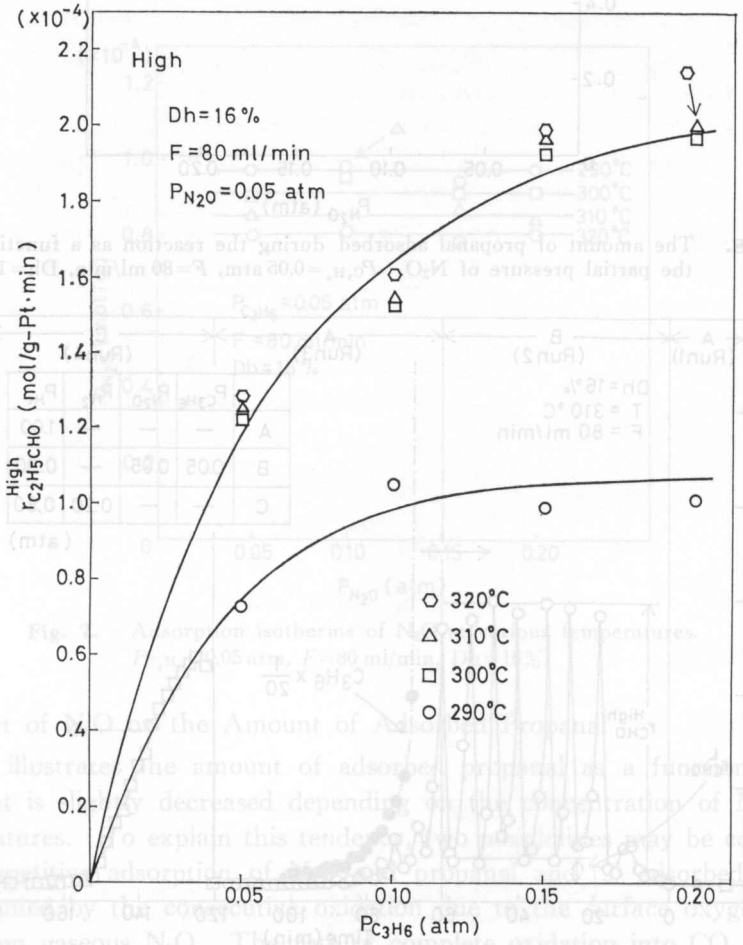

Fig. 10. The rate of propanal formation at the peak of oscillation as a function of $P_{C_3H_6}$. $T=290\sim320$°C, $P_{N_2O}=0.05$ atm, $F=80$ ml/min, Dh=16%.

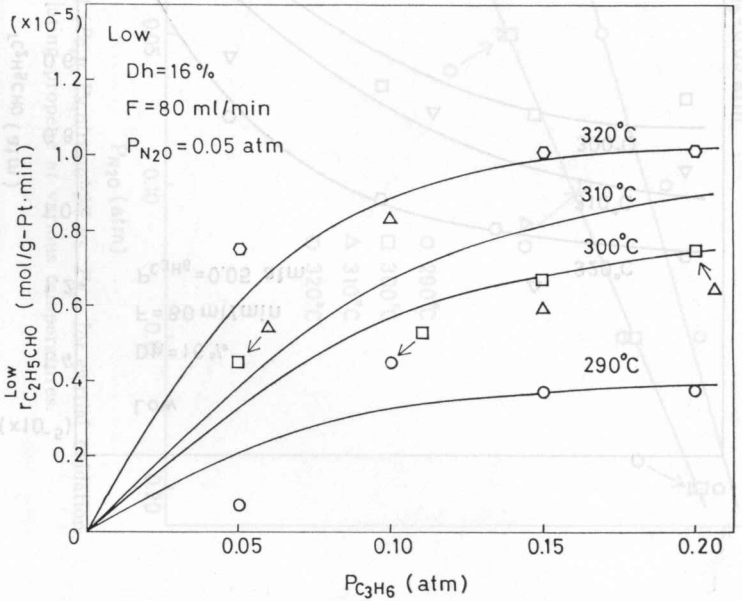

Fig. 11. The rate of propanal formation at the bottom of oscillation as a function of $P_{C_3H_6}=0.05$ atm, $F=80$ ml/min, Dh=16%.

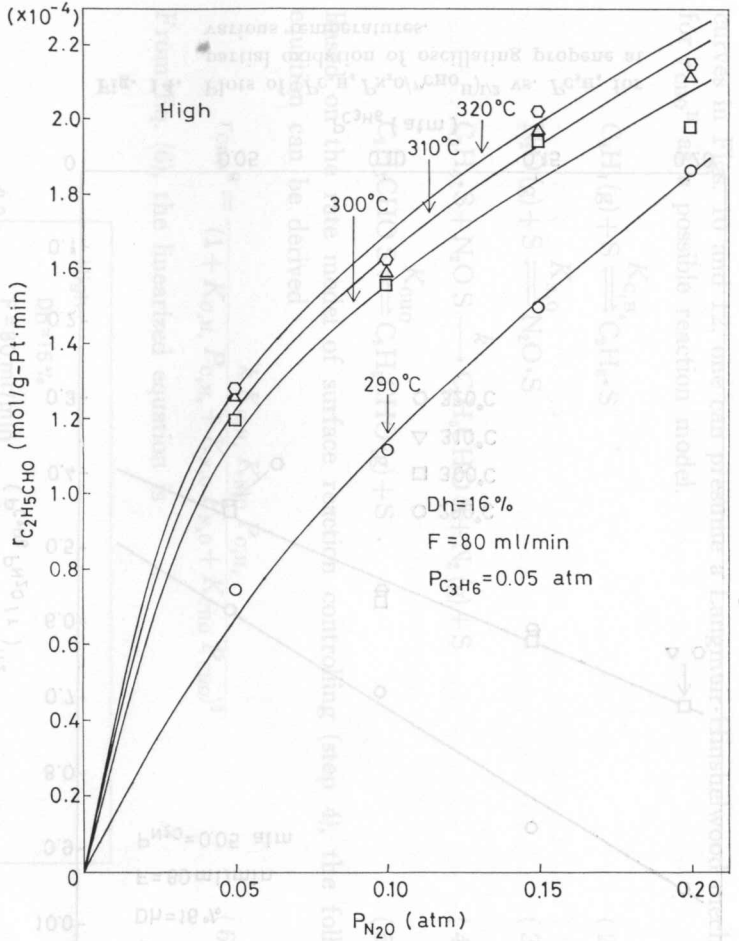

Fig. 12. The rate of propanal formation at the peak of oscillation as a function of P_{N_2O}. $T=290\sim320$°C, $P_{C_3H_6}=0.05$ atm, $F=80$ ml/min, Dh=16%.

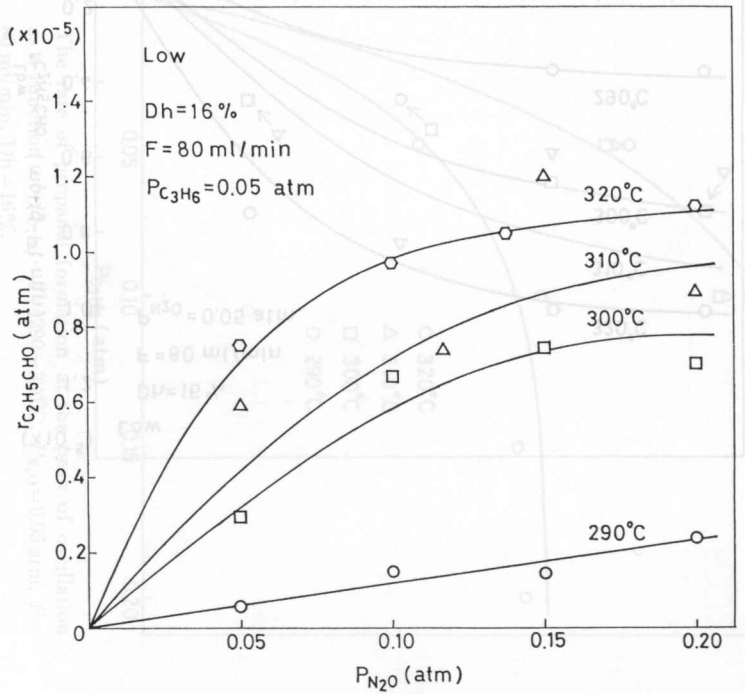

Fig. 13. The rate of propanal formation at the bottom of oscillation as a function of P_{N_2O}. T=290~320°C, $P_{C_3H_6}$=0.05 atm, F=80 ml/min, Dh=16%.

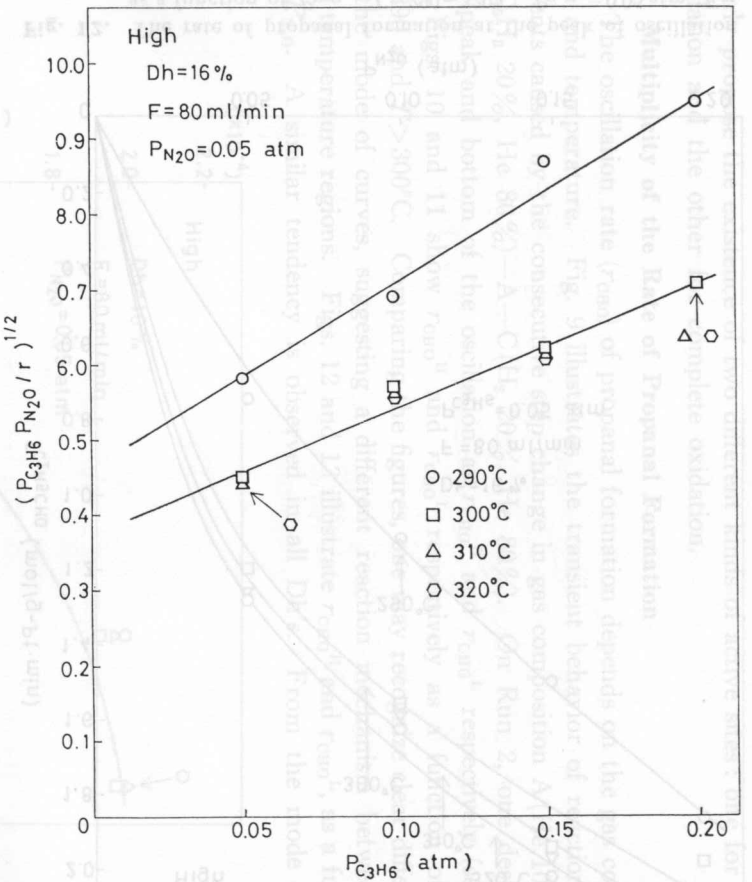

Fig. 14. Plots of $(P_{C_3H_6} P_{N_2O}/r_{CHO}{}^{H})^{1/2}$ vs. $P_{C_3H_6}$ for partial oxidation of oscillating propene at various temperatures.

curves in Figs. 10 and 12, one can presume a Langmuir-Hinshelwood mechanism for $r_{CHO}{}^{H}$ as a possible reaction model.

$$C_3H_6(g)+S \overset{K_{C_3H_6}}{\rightleftharpoons} C_3H_6\cdot S \tag{2}$$

$$N_2O(g)+S \overset{K_{N_2O}}{\rightleftharpoons} N_2O\cdot S \tag{3}$$

$$C_3H_6\cdot S+N_2O\,S \xrightarrow{k} C_2H_5CHO\,S+N_2(g)+S \tag{4}$$

$$C_2H_5CHO\,S \overset{K_{CHO}}{\rightleftharpoons} C_2H_5CHO(g)+S \tag{5}$$

Based on the rate model of surface reaction controlling (step 4), the following equation can be derived

$$r_{CHO}{}^{H}=\frac{k\,K_{C_3H_6}\,K_{N_2O}\,P_{C_3H_6}}{(1+K_{C_3H_6}\,P_{C_3H_6}+K_{N_2O}\,P_{N_2O}+K_{CHO}\,P_{CHO})^2} \tag{6}$$

From Eq. (6), the linearized equation is

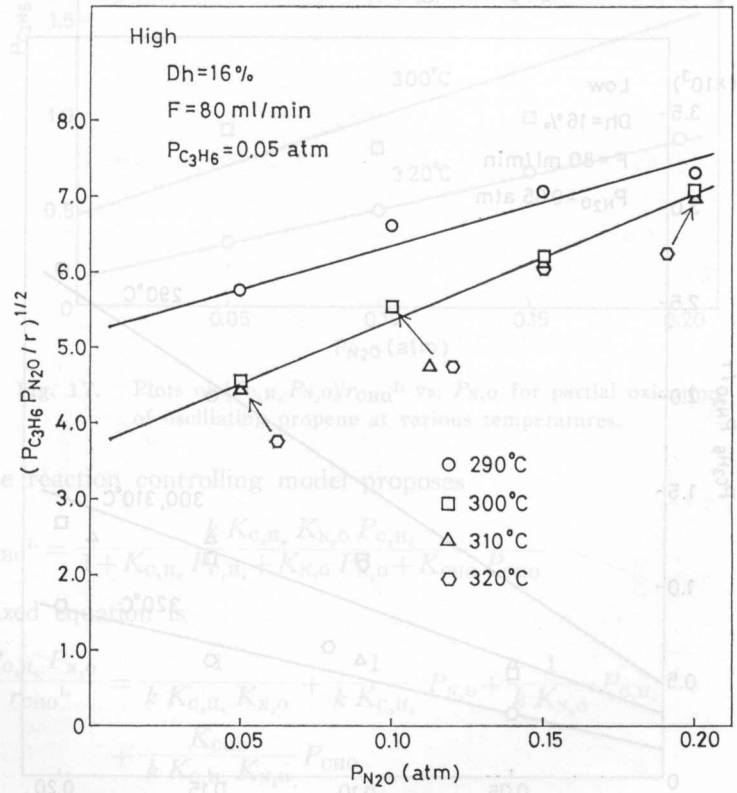

Fig. 15. Plots of $(P_{C_3H_6}P_{N_2O}/r_{CHO}{}^{L})^{1/2}$ vs. P_{N_2O} for partial oxidation of oscillating propene at various temperatures.

$$\left(\frac{P_{C_3H_6}P_{N_2O}}{r_{CHO}{}^{H}}\right)^{1/2}=\frac{1}{(k\,K_{C_3H_6}K_{N_2O})^{1/2}}+\frac{K_{C_3H_6}}{(kK_{C_3H_6}K_{N_2O})^{1/2}}P_{CH}$$
$$+\frac{K_{N_2O}}{(k\,K_{C_3H_6}K_{N_2O})^{1/2}}P_{N_2O}+\frac{K_{CHO}}{(k\,K_{C_3H_6}K_{N_2O})^{1/2}}P_{CHO} \quad (7)$$

Figs. 14 and 15 show the plots of $(P_{C_3H_6}P_{N_2O}/r_{CHO}{}^{H})^{1/2}$ vs. $P_{C_3H_6}$ and P_{N_2O}, respectively. The linear least squares procedure for the model was carried out for the isothermal data.

From the mode of the curves presented in Figs. 11 and 13, an Eley-Rideal model for $r_{CHO}{}^{L}$ may be proposed as follows.

$$C_3H_6(g)+S \overset{K_{C_3H_6}}{\rightleftharpoons} C_3H_6\cdot S \quad (8)$$

$$N_2O(g)+S \overset{K_{N_2O}}{\rightleftharpoons} N\,O\cdot S \quad (9)$$

$$N_2O(g)+C_3H_6\,S \overset{k}{\longrightarrow} C_2H_5CHO\cdot S+N_2(g) \quad (10)$$

$$C_2H_5CHO\cdot S \overset{K_{CHO}}{\rightleftharpoons} C_2H_5CHO(g)+S \quad (11)$$

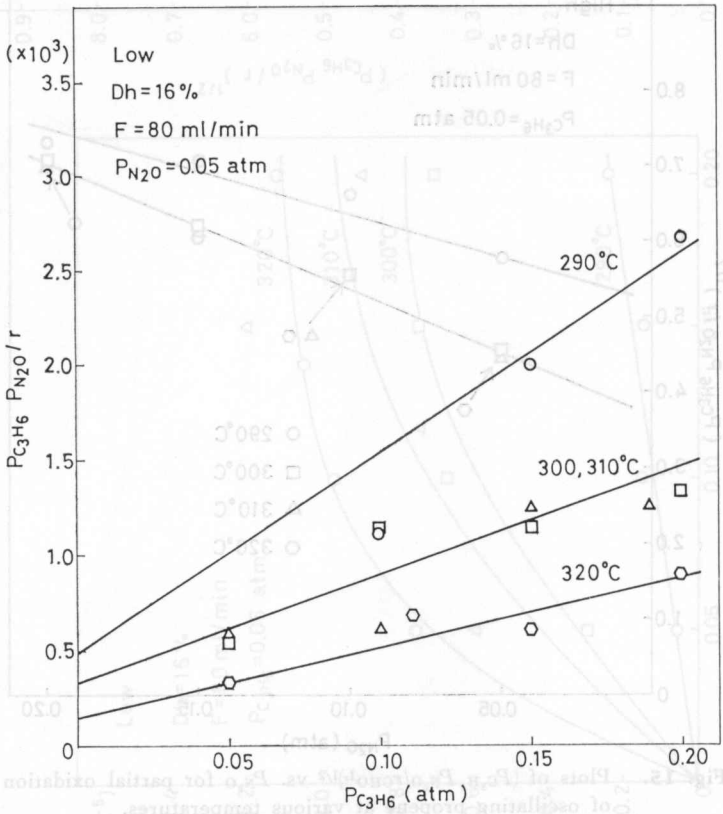

Fig. 16. Plots of $(P_{C_3H_6}P_{N_2O})/r_{CHO}{}^{L}$ vs. $P_{C_3H_6}$ for partial oxidation of oscillating propene at various temperatures.

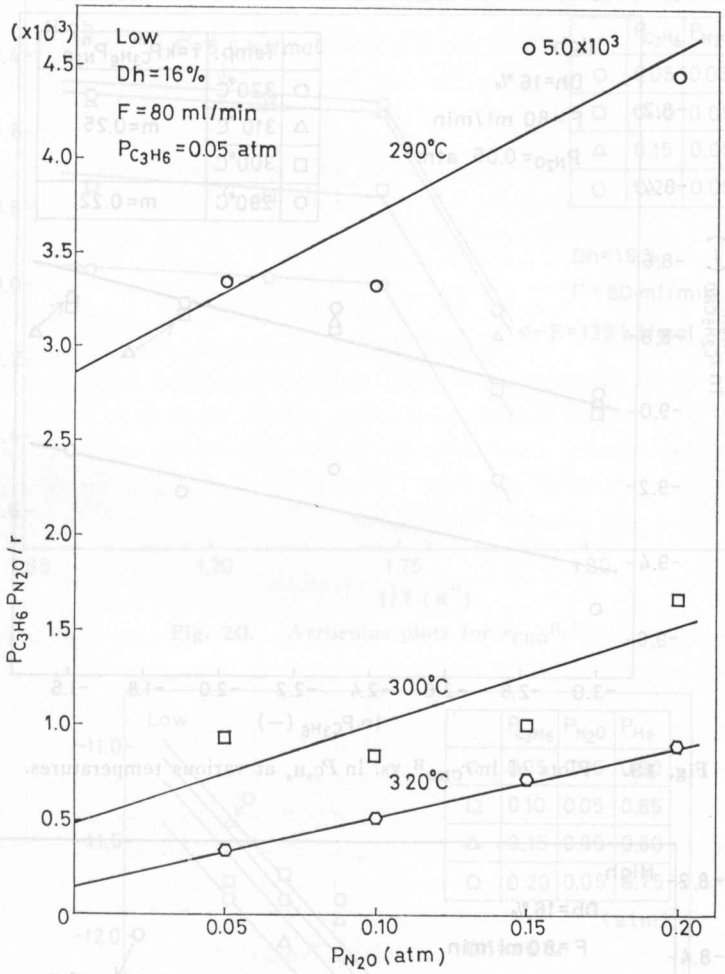

Fig. 17. Plots of $(P_{C_3H_6}P_{N_2O})/r_{CHO}{}^{L}$ vs. P_{N_2O} for partial oxidation of oscillating propene at various temperatures.

The surface reaction controlling model proposes

$$r_{CHO}{}^{L}=\frac{k\,K_{C_3H_6}K_{N_2O}P_{C_3H_6}}{1+K_{C_3H_6}P_{C_3H_6}+K_{N_2O}P_{N_2O}+K_{CHO}P_{CHO}} \tag{12}$$

The linearized equation is

$$\frac{P_{C_3H_6}P_{N_2O}}{r_{CHO}{}^{L}}=\frac{1}{k\,K_{C_3H_6}K_{N_2O}}+\frac{1}{k\,K_{C_3H_6}}P_{N_2O}+\frac{1}{k\,K_{N_2O}}P_{C_3H_6}+\frac{K_{CHO}}{k\,K_{C_3H_6}K_{N_2O}}P_{CHO} \tag{13}$$

Figs. 16 and 17 show the plots of $(P_{C_3H_6}P_{N_2O})/r_{CHO}{}^{L}$ vs. $P_{C_3H_6}$ and P_{N_2O}, respectively. The results obtained indicate a rough linear relation suggesting a suitable model.

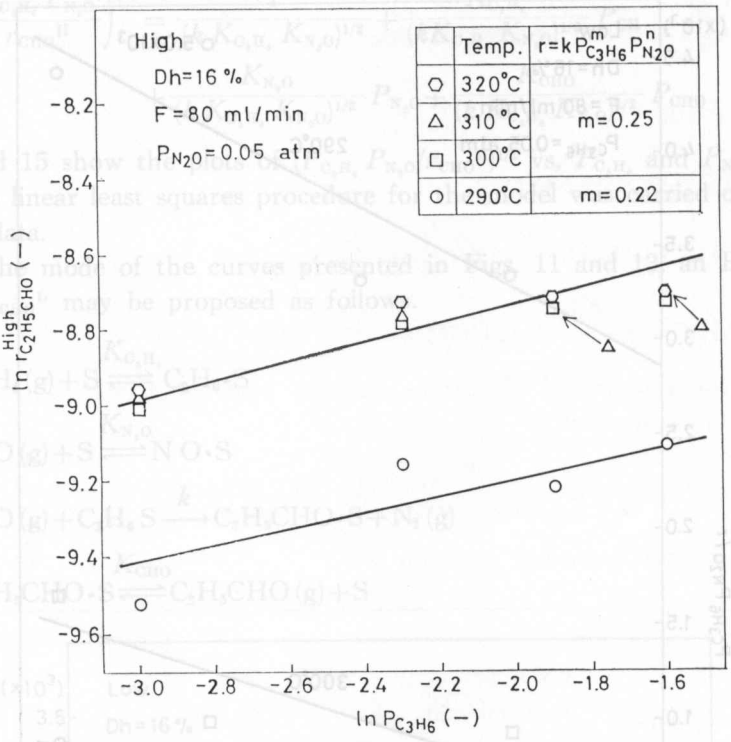

Fig. 18. Plots of $\ln r_{CHO}{}^{H}$ vs. $\ln P_{C_3H_6}$ at various temperatures.

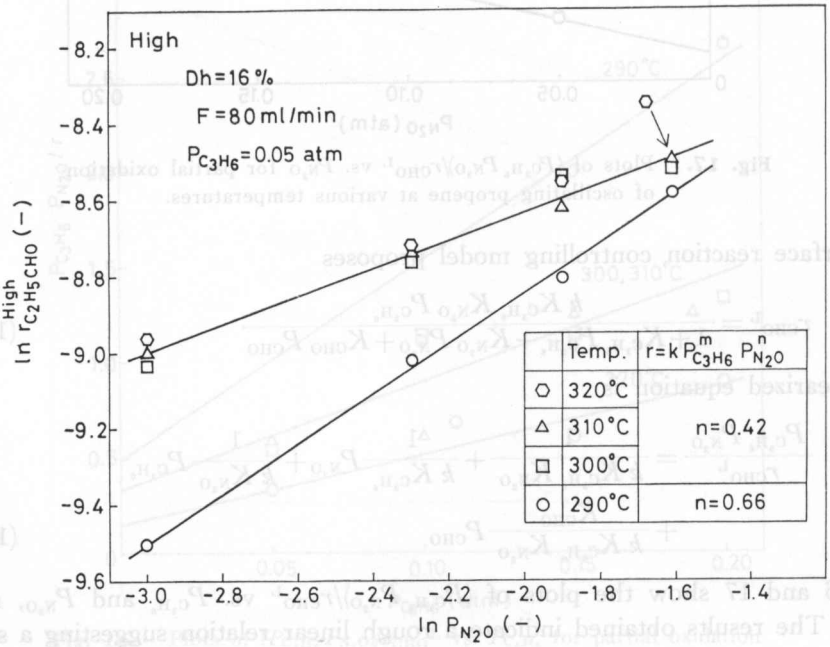

Fig. 19. Plots of $\ln r_{CHC}{}^{H}$ vs. $\ln P_{N_2O}$ at various temperatures.

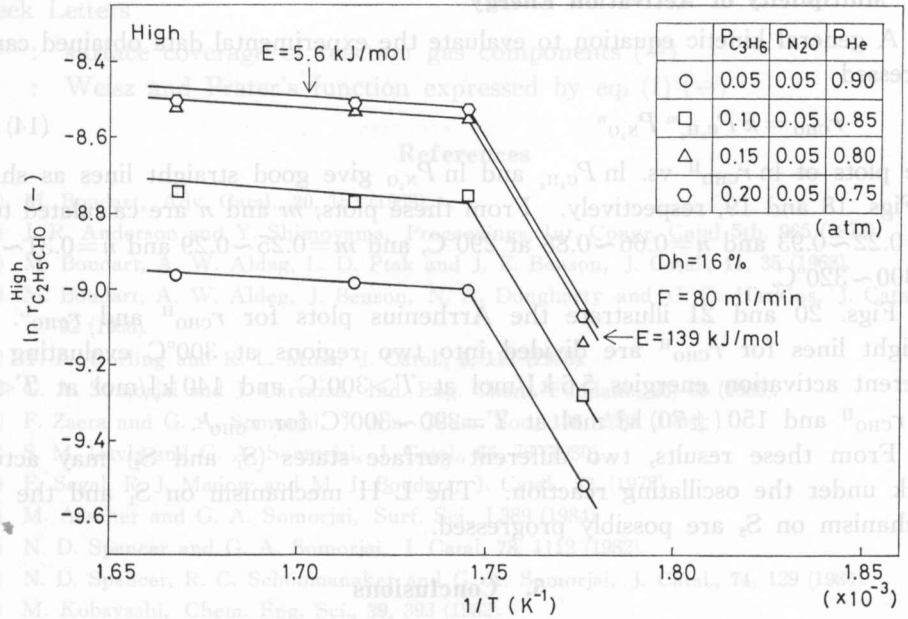

Fig. 20. Arrhenius plots for $r_{CHO}{}^{H}$.

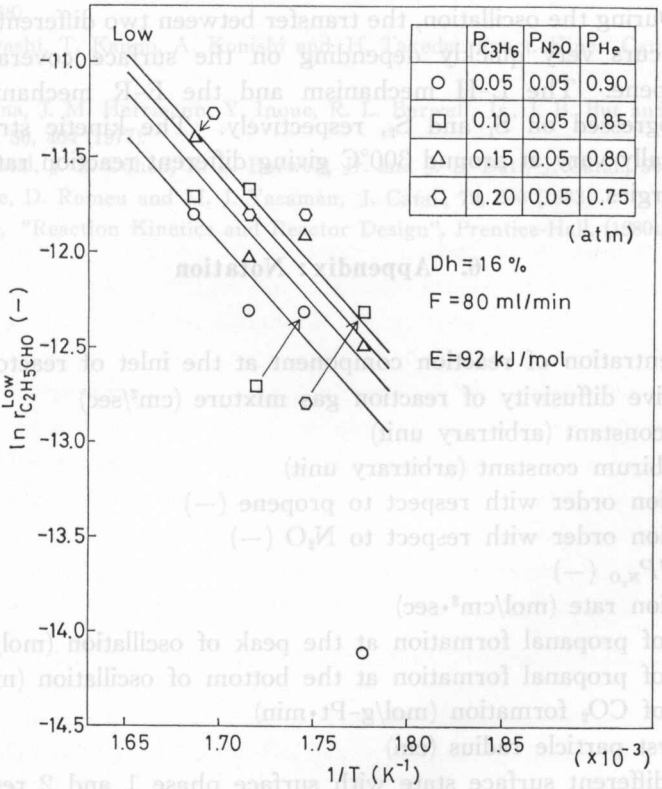

Fig. 21. Arrhenius plots for $r_{CHO}{}^{L}$.

4-5. Multiplicity of Activation Energy

A general kinetic equation to evaluate the experimental data obtained can be expressed

$$r_{CHO} = k P_{C_3H_6}{}^m P_{N_2O}{}^n \quad (14)$$

The plots of $\ln r_{CHO}{}^H$ vs. $\ln P_{C_3H_6}$ and $\ln P_{N_2O}$ give good straight lines as shown in Figs. 18 and 19, respectively. From these plots, m and n are calculated to be $m=0.22\sim0.93$ and $n=0.66\sim0.88$ at 290°C, and $m=0.25\sim0.29$ and $n=0.31\sim0.42$ at $300\sim320$°C.

Figs. 20 and 21 illustrate the Arrhenius plots for $r_{CHO}{}^H$ and $r_{CHO}{}^L$. All straight lines for $r_{CHO}{}^H$ are divided into two regions at 300°C evaluating two different activation energies 5.6 kJ/mol at $T>300$°C and 140 kJ/mol at $T<300$ for $r_{CHO}{}^H$ and 150 ($\pm$70) kJ/mol at $T=290\sim300$°C for $r_{CHO}{}^L$.

From these results, two different surface states (S_1 and S_2) may actually work under the oscillating reaction. The L-H mechanism on S_1 and the E-R mechanism on S_2 are possibly progressed.

5. Conclusions

The platinum surface during the oxidation of propene is extremely mobile at $290\sim320$°C, exhibiting an oscillatory rate of propanal formation not CO_2 formation. During the oscillation, the transfer between two different surface states S_1 and S_2 occurs very quickly depending on the surface coverage of weakly adsorbed propene. The L-H mechanism and the E-R mechanism are independently progressed on S_1 and S_2, respectively. The kinetic structures on S_1 and S_2 drastically vary at around 300°C giving different reaction rate kinetics and activation energies.

6. Appendix: Notation

Symbols

Co : concentration of reaction component at the inlet of reactor (mol/cm^3)
D_{eff} : effective diffusivity of reaction gas mixture (cm^2/sec)
k_j : rate constant (arbitrary unit)
K_j : equilibirum constant (arbitrary unit)
m : reaction order with respect to propene (−)
n : reaction order with respect to N_2O (−)
R : $P_{C_3H_6}/P_{N_2O}$ (−)
r : reaction rate (mol/cm^3•sec)
$r_{CHO}{}^H$: rate of propanal formation at the peak of oscillation (mol/g-Pt•min)
$r_{CHO}{}^L$: rate of propanal formation at the bottom of oscillation (mol/g-Pt•min)
r_{CO_2} : rate of CO_2 formation (mol/g-Pt•min)
R_p : catalyst particle radius (cm)
S_1, S_2 : two different surface state with surface phase 1 and 2 respectively. (−)

Greek Letters

θ_j : surface coverage of reaction gas components (−)

Φ : Weisz and Prater's function expressed by eq. (1) (−)

References

1) M. Boudart, Adv. Catal., **20**, 153 (1969).
2) J. R. Anderson and Y. Shimoyama, Proceedings, Int. Congr. Catal 5th, 965 (1973).
3) M. Boudart, A. W. Aldag, L. D. Ptak and J. E. Benson, J. Catal., **11**, 35 (1968).
4) M. Boudart, A. W. Aldeg, J. Benson, N. A. Dongharty and G. C. Harkins, J. Catal., **6**, 92 (1966).
5) T. A. Dorling and R. L. Moss, J. Catol., **5**, 111 (1966).
6) G. A. Somorjai and J. Carrazza, Ind. Eng. Chem. Fundam., **25**, 63 (1986).
7) F. Zaera and G. A. Somorjai, J. Am. Chem. Soc., **106**, 2288 (1984).
8) S. M. Davis and G. A. Somorjai, J. Catal., **65**, 78 (1980).
9) E. Segal, R. J. Madow and M. J. Boudart, J. Catal., **52**, (1978)
10) M. Asscher and G. A. Somorjai, Surf. Sci., L389 (1984).
11) N. D. Spencer and G. A. Somorjai, J. Catal, **78**, 1112 (1982).
12) N. D. Spencer, R. C. Schoomanaker and G. A. Somorjai, J. Catal., **74**, 129 (1984).
13) M. Kobayashi, Chem. Eng. Sci., **39**, 393 (1982).
14) C. O. Bennett, Catal. Rev. Eng. Sci., **12**, 105 (1976).
15) H. Takeda, T. Kanno and M. Kobayashi, Memoir of Kitami Institute of Technology, **20**, 21 (1988).
16) M. Kobayashi, T. Kanno, A. Konishi and H. Takeda, React. Kinet. Catal. Letter., **37**, 89 (1988).
17) T. Uchijima, J. M. Herrmann, Y. Inoue, R. L. Burwell, Jr., J. B. But and J. B. Cohen, J. Catal., **50**, 464 (1977).
18) S. R. Sashtal, J. B. Cohen, R. L. Burwell, Jr. and J. B. Butt, J. Catal., **50**, 479 (1977).
19) O. L. Pere, D. Romeu and M. J. Yacaman, J. Catal., **79**, 240 (1983).
20) J. B. Butt, "Reaction Kinetics and Reactor Design", Prentice-Hall, (1980).